From Cradle To Grave: The Rise and Demise of the Comets

David C. Jewitt

Institute for Astronomy, University of Hawaii, 2680 Woodlawn Drive, Honolulu, HI 96822, USA

Abstract. The active comets are a dynamic ensemble of decaying bodies, recently arrived from cold storage locations in the Kuiper Belt and Oort Cloud. In this chapter, we discuss the processes that drive the physical transformation and decay of cometary nuclei as they move from the frigid outer regions into the hot environment of the inner Solar system.

For COMETS II: Eds. M. Festou, H. Weaver, H. U. Keller

1 Introduction

In this chapter, we discuss the processes that drive the physical transformation and decay of cometary nuclei as they move from the frigid outer regions into the hot environment of the inner Solar system. Fundamentally, comets and asteroids are distinguished by their volatile content, which is itself a measure of the temperature of the environment in which they accreted. Comets possess a substantial fraction of bulk water ice that is not expected in the asteroids of the main-belt (Whipple 1950 thought comets might contain a water ice fraction near 50% by mass but recent data suggest smaller fractions. Reach et al (2000), for example, estimate a ratio 3% to 10% in 2P/Encke while Grün et al (2001) find that only 10% to 15% of the mass lost from C/hale-Bopp was from sublimated ice). Unfortunately, we possess no direct way to measure the bulk fraction of water ice within any nucleus or asteroid. The fundamental distinction between comets and asteroids is not reflected in any clean-cut, practical means by which to distinguish them.

Instead, the widely applied practical definition is that a comet is defined by showing a resolved coma at some point in its orbit. Deciding whether an object is an asteroid or a comet thus depends critically on the instrumental resolution and sensitivity to low surface brightness coma. A weakly active comet might not be detected as such if observed with insufficient resolution or sensitivity. Thus, there arises a grey zone in which the cometary vs asteroidal nature of a given body cannot easily be ascertained by observations.

A third distinction between asteroids and comets may be drawn based on the respective dynamical properties. The Tisserand invariant with respect to Jupiter is a popular discriminant. It is defined by

$$T_J = \frac{a_J}{a} + 2\left((1-e^2)\frac{a}{a_J}\right)^{1/2} cos(i) \quad (1)$$

where a, e and i are the semimajor axis, eccentricity and inclination of the orbit while $a_J = 5.2$ AU is the semimajor axis of the orbit of Jupiter. This parameter, which is conserved in the circular, restricted 3-body problem, provides a measure of the relative velocity of approach to Jupiter: Jupiter itself has $T_J = 3$, most comets have $T_J < 3$ while main-belt asteroids generally have $T_J > 3$. Unfortunately, the dynamical definition of comet-hood does not always match the observational or compositional definitions. A number of comets (including the famous 2P/Encke) have asteroid-like $T_J > 3$ while many bodies with comet-like $T_J < 3$ are asteroids scattered from the main-belt. There are other difficult cases: the Jovian Trojan asteroids have $T_J \sim 3$, probably possess ice-rich interiors (and so are comets by the physical definition) but are too cold to sublimate, show no comae and are labelled "asteroids".

Evidently, this is not a clean subject. Even the definition of the term "comet" is arguable, and the reader will see that much of the following discussion will be drawn inexorably towards objects whose cometary nature is debatable. To try to maintain focus we adopt a tutorial style that is intended to highlight connections between seemingly disparate subjects and which deliberately dissects and simplifies complicated problems to make them understandable. Sufficient references are given that the interested reader may take an easy step into the research literature, but we have made no attempt to be complete since the number of relevant publications is already very large. Aspects of this subject have been reviewed elsewhere (Degewij and Cruikshank 1982, Jewitt 1996a, Weissman et al. 2002).

2 Cometary Reservoirs

Comets are observationally defined as Solar system bodies which maintain at least transient gaseous, or dusty, comae. The comae are gravitationally unbound (escaping) atmospheres produced by classical sublimation of near-surface ices in response to heating by the sun. Their small sizes (typically a few km) and resulting short sublimation lifetimes (typically $\sim 10^4$ yrs) guarantee that the observed comets are recent arrivals in the inner Solar system. If a steady state population is to be maintained, the comets must be continually resupplied from one or more long-lived reservoirs.

Two primary reservoirs of the comets, the Oort Cloud and the Kuiper Belt, are now recognized (Figure 1). In the absence of contrary evidence, it is assumed that both are primordial, of age $\tau_{SS} = 4.5 \times 10^9$ yr.

(Timescales mentioned in the text are summarized graphically in Figure 2).

2.1 Oort Cloud

The Oort Cloud was identified first from the peculiar distribution of the semimajor axes of long-period comets (LPCs; Oort 1950). It supplies a nearly isotropic flux of LPCs to the planetary region and is of vast extent, with characteristic length scale $R_{oc} \sim 100{,}000$ AU and orbital periods near $\tau_{oc} \sim 10^6 - 10^7$ yr.

The total number of Oort Cloud comets larger than about 1 km in radius is of order $N_{oc} \sim 10^{12}$ (see the chapters by Rickman and by Dones et al.). Comets now in the Oort Cloud are thought to have originated in the proto-planetary disk between Jupiter and Neptune, while most were scattered out by Uranus and Neptune (Hahn and Malhotra 1999).

The dynamical part of Oort's model predicts a ratio of returning comets relative to first-appearing comets that is larger than is observed. Oort's solution was to introduce a "fading parameter" to diminish the number of returning comets. Ideas about the nature of the fading mechanism range from the sublimation of supervolatile frosting accreted from the interstellar medium to physical disintegration of the nuclei soon after entry into the planetary region. The need for a spherical source to supply the isotropic orbital inclination distribution seems secure, as does the the large effective size of the source (indicated by the large semimajor axes of the LPCs). No plausible alternatives to Oort's model have been found in the 50 years since its introduction (see Wiegert and Tremaine 1999). Still, the uncertain nature of the fading parameter on which its success depends remains disconcerting.

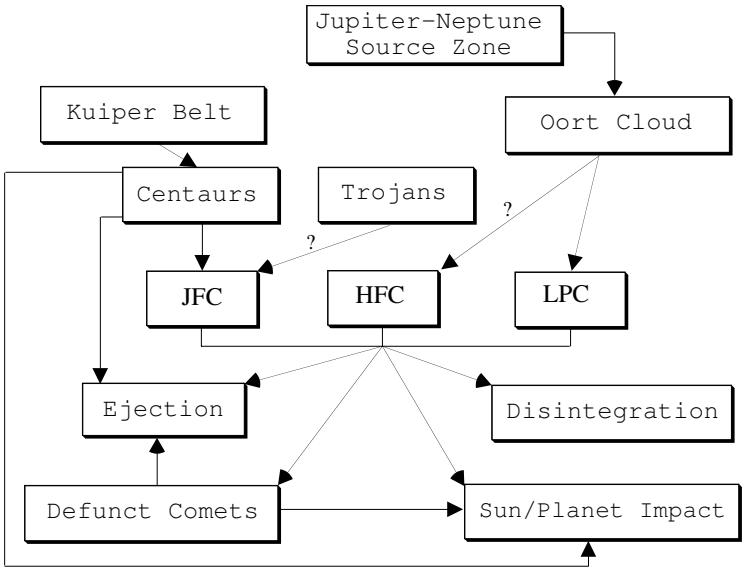

Fig. 1. Current interrelations among the planetary small body populations. JFC = Jupiter Family Comet, HFC = Halley Family Comet, LPC = Long Period Comet (also known as Isotropic Source comets). Question marks indicate the uncertain path from the Oort Cloud to the HFCs and the unknown contribution to the JFCs from the Trojans of the giant planets. The defunct comets include both dead (totally devolatilized) and dormant (volatiles shielded from Solar insolation) bodies. Adapted from Jewitt and Fernández (2001).

The collision time in the Oort Cloud is $\tau_c \sim \tau_{oc}/\gamma$, where γ is the optical depth, equal to the ratio of the sum of the cross-sections of the constituent nuclei to the effective geometric cross-section of the cloud. We write

$$\gamma \sim N_{oc} \left(\frac{r_n}{R_{oc}} \right)^2 \tag{2}$$

where r_n is the effective nucleus radius. We assume that the cross-section is dominated by the smallest objects and take $r_n = 1$ km. Substitution gives $\gamma \sim 10^{-14}$ and, with $\tau_{oc} \sim 10^7$ yr, we find that $\tau_c >> \tau_{SS}$ and so is effectively infinite. Any collisional processing of the Oort Cloud comets must have occurred at early times, prior to their emplacement in distant heliocentric orbits (Stern and Weissman 2001).

2.2 Halley Family Comets

The Halley Family Comets (HFCs, also known as Halley Type Comets) are a separate group distinguished by having short orbital periods but a wide spread of inclinations, including retrograde orbits that are absent in the Jupiter Family. These bodies have Tisserand parameters (Eq. 1) $T_J < 2$. The prototype 1P/Halley ($a = 17.8$ AU, $e = 0.97$, $i = 162$ deg, T_J = -0.61) is typical. They are thought to derive from the inner Oort Cloud by gravitational capture, principally by interaction with the massive gas giant planets (Bailey and Emelyanenko 1996, Levison et al. 2001, Rickman et al. 2002). However, the details of this capture and their implications for the structure of the inner Oort Cloud are controversial. The HFCs follow a complex dynamical evolution under the control of mean-motion and secular resonances, ending with ejection from the planetary system or impact with the sun after a mean time of order 10^6 yr (Bailey and Emelyanenko 1996). These objects are rare compared to Jupiter Family comets in the observational sample only because there is a strong observational bias against them. In absolute numbers, the HFCs may outnumber the Jupiter Family by a large factor.

2.3 Kuiper Belt, Centaurs and Jupiter Family Comets

The Jupiter family comets (JFCs) occupy small orbits with modest inclinations and eccentricities. Their Tisserand parameters are $2 \leq T_J < 3$ (Levison 1996). Most JFCs probably originate from a trans-Neptunian source known as the Kuiper Belt (Fernández 1980, Duncan et al. 1988), whose inclination distribution is similar to that of the JFCs themselves. In this scenario, the kilometer-sized JFCs could be collisionally produced fragments of larger Kuiper Belt Objects (Stern 1995, Farinella and Davis 1996, see chapter by Duncan et al.). The representative orbital period in the Kuiper Belt is $\tau_{KB} \sim 10^2 - 10^3$ yr.

The number of Kuiper Belt comets larger than 1 km radius, N_1, is crucial if the Kuiper Belt is to supply the JFCs. However, this number is highly uncertain. Early estimates based on extrapolation from 100 km scale KBOs gave $N_1 \sim 10^{10}$ (Jewitt et al. 1998). The first direct measurements of ∼10 km scale KBOs in the classical region of the belt, when extrapolated to 1 km, give $N_1 \sim 10^8$ (Bernstein et al. 2003), which may be too small for the classical belt to supply the JFCs. However, the number of Scattered KBOs remains observationally unconstrained at small sizes, and this population could supply the JFCs for the age of the Solar system.

The Centaurs are dynamically intermediate between the Kuiper Belt and the Jupiter Family Comets. We here define Centaurs as objects with perihelia $q > a_J$ and semimajor axes $a < a_N$, where $a_J = 5.2$ AU and $a_N = 30$ AU are the semimajor axes of Jupiter and Neptune, respectively (Jewitt and Kalas 1998). By this definition, there are currently (October 2002) 42 known Centaurs, including the prototype 2060 Chiron, also known as 95P/Chiron ($a = 13.6$ AU, $e = 0.38$, $i = 15$ deg). Most appear asteroidal but five have been observed to show comae and thus are also properly recognized as comets (Table 1). A further 140 known objects dip into the planetary region from the Kuiper Belt and beyond (i.e. $q \leq a_N$ and $a > a_N$).

Table 1. The Known Cometary Centaurs

Object	Perihelion [AU]	Semimajor Axis [AU]	Eccentricity	Inclination [deg]	Tisserand Parameter
C/2001 M10	5.30	26.66	0.80	28.0	2.59
29P/SW1	5.72	5.99	0.04	9.4	2.98
39P/Oterma	6.83	7.25	0.24	1.9	3.01
2060 Chiron	8.45	13.62	0.38	6.9	3.36
C/2001 T4	8.56	13.92	0.38	15.4	3.29

Once trapped as Centaurs the dynamical lifetimes are limited by strong gravitational scattering by the giant planets to $\tau_{Cen} \approx 10^7$ yr (Dones et al. 1999). Most Centaurs are ejected from the Solar system. The survivors that become trapped inside Jupiter's orbit tend to sublimate and are observationally relabelled as JFCs. Their median dynamical lifetime (Levison and Duncan 1994) is $\tau_{JFC} = 3.3 \times 10^5$ yr. Note that the dynamical evolution is chaotic and the reverse transition from JFC to Centaur is common (as happened recently with comet/Centaur 39P/Oterma).

The comets follow chaotic trajectories amongst the planets (with dynamical memories ∼ 1000 yrs, Tancredi 1995), and elaborate numerical models must be used to track their orbital evolution (Levison and Duncan 1994, 1997). Very roughly, the probability that a comet or Centaur will be scattered inwards following its encounter with a planet is $p \sim 1/2$. This means that the fraction of the escaped KBOs that are scattered inwards by Neptune is just p, while the

fraction that scatter between the four giant planets down past Jupiter is $p^4 \sim 0.05$. If we assume that the KBOs have an effective lifetime comparable to τ_{SS}, then the steady state population of the Centaurs, N_{Cen}, relative to that of the KBOs, N_{KBO}, may be crudely estimated from

$$\frac{N_{Cen}}{N_{KBO}} \sim p \left(\frac{\tau_{Cen}}{\tau_{SS}} \right) \sim 10^{-3}. \quad (3)$$

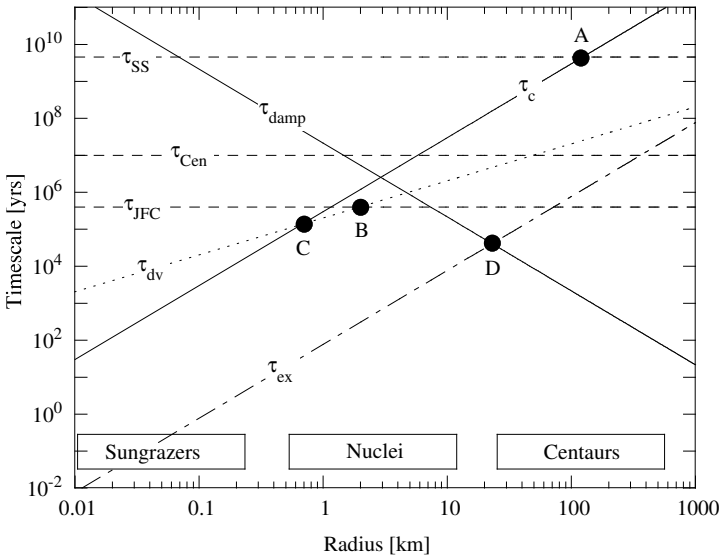

Fig. 2. Timescales relevant to the cometary nucleus. The representative size ranges of the well-measured sungrazers, JFC nuclei and Centaurs are shown as separate for clarity: in fact, their size ranges overlap. Labelled curves and lettered points are described in the text. Lines for τ_{dv} and τ_{ex} refer to outgassing from comets at $a = 3.5$ AU. Adapted from Jewitt (1996a).

With $N_{KBO} \sim 70{,}000$ (diameters $D > 100$ km, Jewitt et al. 1998, Trujillo et al. 2001), this gives $N_{Cen} \sim 70$, in good agreement with observational estimates of $N_{Cen} \sim 100$ measured to the same size (Sheppard et al. 2000).

In the same spirit of approximation, the steady state population of the JFCs is given by

$$\frac{N_{JFC}}{N_{KBO}} \sim p^4 \left(\frac{\tau_{JFC}}{\tau_{SS}} \right) \sim 5 \times 10^{-6}. \quad (4)$$

This leads us to expect in steady state ~ 0.4 JFCs of diameter $D \geq 100$ km, consistent with the observation that there are currently none. The number of

KBOs with $D \geq 100$ km is $N_{KBO} \sim 7{\times}10^4$ based on a simple extrapolation from survey data (Jewitt et al. 1998). The number of KBOs with $D \geq 1$ km is very uncertain because an extrapolation of the size distribution must be made. A current best-guess population is $N_{KBO} \sim$ (1 to 10) $\times 10^9$ (but see Bernstein et al. 2003). With Eq. (4), this gives $5,000 \leq N_{JFC} \leq 50{,}000$. Although very uncertain, the lower end of this range is comparable to the (equally uncertain) "several thousand to about 10^4" JFCs observationally estimated by Fernández et al. (1999, see also Delsemme 1973). A more detailed estimate should include, in addition to a proper treatment of the dynamics, a correction for the loss of JFC nuclei through such processes as devolatization and disruption. A numerical treatment by Levison and Duncan (1997) finds that the source region of the JFCs must contain $7{\times}10^9$ objects, in agreement with early estimates but larger than the number of appropriately sized KBOs in the Classical Belt. A significant problem in comparing source models with population measurements is that the sizes of the objects being compared (cometary nuclei vs. KBOs) are not well determined because the albedos are not well known.

2.4 Other Sources of Comets

The distributions of color (Jewitt and Luu 1990) and albedo (Fernández et al. 2003) of the Jovian Trojan 'asteroids' are formally indistinguishable from those of the cometary nuclei. This suggests (but does not prove) an intriguing compositional similarity between the two classes of body, at least at the surface level where irradiation and Solar heating may play a role. No ices have been spectroscopically detected on the Trojans (Jones et al. 1990, Luu et al. 1994, Dumas et al. 1998) but this is not surprising given the high surface temperatures ($\sim$ 150 K) and the expected rapid loss of exposed ice by sublimation. Beneath their refractory mantles, however, the Trojans may be ice rich. They may contribute to the comet population through dynamical instabilities and collisional ejection (Marzari et al. 1995). Once removed from the vicinity of the Lagrangian L4 and L5 points, they quickly lose dynamical traces of their origin. There are too few Jovian Trojans to supply more than $\sim$10% of the flux of JFCs (Marzari et al. 1995, Jewitt et al. 2000), but Trojans of the other giant planets, if they exist, could be significant additional sources, and the total flux of escaped Trojans from all giant planets should be considered unknown. A narrow ring of orbits between Uranus and Neptune may be another source (Holman 1997) although these orbits may not remain populated if the outer planets experienced substantial radial migration (Brunini and Melita 1998).

3 Onset of Activity

Equilibrium surface temperatures in the cometary reservoirs are low ($\sim$ 10 K in the Oort Cloud and $\sim$ 40 K in the Kuiper Belt). As orbital evolution carries the comets closer to the sun, rising temperatures induce the sublimation of surface volatiles. The first abundant ice to sublimate is the highly volatile carbon

monoxide, CO, which is thought to produce the comae observed around some Centaurs in the middle Solar system ($R \sim 10$ AU, Table 1, Figure 3). However, most Centaurs show no comae (e.g. Figure 4), either because they have already lost their near-surface volatiles through outgassing or because their surfaces consist of non-volatile, complex organic and silicate mantles produced by energetic particle bombardment (see chapter by Barucci et al). Although CO is the most volatile abundant ice in comets, the main driver of activity inside ∼5 AU, as recognised long ago by Whipple (1950), is the sublimation of water ice, beginning near the orbital radius of Jupiter.

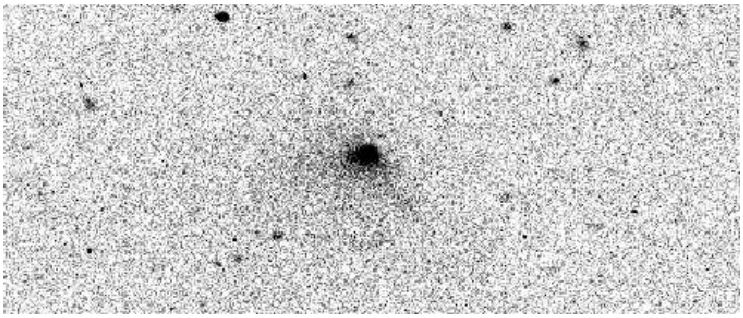

Fig. 3. Cometary Centaur C/2001 T4 in a 300 sec., R-band image taken by the author using the University of Hawaii 2.2-m telescope on UT 2002 September 4. The heliocentric and geocentric distances were $R = 8.57$ AU and $\Delta = 7.97$ AU, respectively, and the phase angle was 5.6 deg. Image is 96 arcsec wide and has North at the top, East to the left.

Solar heat propagates into the interior of the nucleus. The timescale for the conduction of heat to the center of a spherical nucleus of radius r_n is given by solution of the conduction equation

$$k\nabla^2 T(r,t) = \rho c_p \frac{dT(r,t)}{dt} - \rho H(r,t) \tag{5}$$

where $T(r,t)$ is the temperature as a function of radius and time, k is thermal conductivity, ρ is bulk density, c_p is the specific heat capacity and $H(r,t)$ is the specific power production due to internal heat sources (e.g. radioactivity, phase transitions). Dimensional treatment of this equation gives the characteristic e-folding timescale for heat transport by conduction as

$$\tau_c \sim \left(\frac{r_n^2}{\kappa} \right) \tag{6}$$

where $\kappa = k/(\rho c_p)$ is the thermal diffusivity. For a nominal thermal diffusivity $\kappa = 10^{-7}\ m^2 s^{-1}$, we have

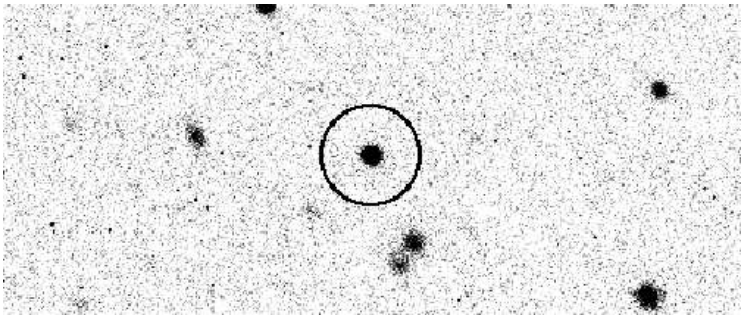

Fig. 4. Centaur 1998 SG_{35} in a 900 sec., R-band image taken by the author using the University of Hawaii 2.2-m telescope on UT 2002 September 8. The heliocentric and geocentric distances were $R = 8.72$ AU and $\Delta = 8.12$ AU, respectively, and the phase angle was 5.5 deg. Image has the same orientation and scale as Figure 3. In sharp contrast to C/2001 T4 (Figure 3), this Centaur shows no coma or tail when observed at a nearly identical heliocentric distance and for a longer time.

$$\tau_c \sim 3 \times 10^5 r_n^2 \text{ yr} \tag{7}$$

with r_n expressed in km. Setting $\tau_c = \tau_{SS}$ gives $r_n \sim 100$ km as the maximum size for effective conductive heat transport (Figure 2, point A). All known cometary nuclei, but not the Centaurs or KBOs, are smaller than this. Note that $\tau_c > \tau_{JFC}$ for $r_n > 1$ km, meaning that the deep interiors of the nuclei of most JFCs are effectively thermally decoupled from their surfaces.

4 Effects of Activity

Mass loss due to sublimation can exert a profound influence on the physical nature of the cometary nucleus, perhaps changing the shape, the size, the rotation and even the survival time in the inner Solar system. Furthermore, these effects are likely interrelated. Anisotropic, mass-loss produces torques on the nucleus that change the spin and the nucleus shape, leading to a change in the distribution of active areas and in the torque. Centripetal effects may lead to loss of material from the rotational equator, affecting the size, shape, spin and mantling. For clarity of preentation, these effects are discussed separately here, but they are in reality closely intertwined.

4.1 Mantle Formation

The existence of refractory surface mantles is suggested by ground-based observations of many comets (A'Hearn et al. 1995) and by direct imaging of the nuclei of comets 1P/Halley and 19P/Borrelly at subkilometer resolution. The observations show that sublimation of cometary volatiles is restricted to active

areas occupying a fraction of the surface area $10^{-3} \leq f \leq 10^{-1}$. (larger active fractions $\sim$1 are sometimes reported, but these may reflect gas production from secondary sources in an icy grain halo about the nucleus; Lissé et al. (1999)). The corresponding f for the nuclei of long-period comets is observationally not well established. The inactive regions correspond to volatile-depleted surface thought to consist of refractory crust or mantle material. Many comets with $f << 10^{-3}$ cannot be easily distinguished from asteroids owing to the practical difficulty of detecting very weak dust (Luu and Jewitt 1992a) or gas comae (Chamberlin et al. 1996).

In the so-called rubble mantle model, the mantles are thought to consist of refractory blocks that are too large to be ejected by gas drag against the gravity of the nucleus. Such mantles need only be thicker than the thermal skin depth ($L_D \sim (\kappa P_{rot})^{1/2}$ where P_{rot} is the nucleus rotation period), in order to inhibit sublimation. For representative values $P_{rot} = 6$hr, $\kappa = 10^{-7} m^2 s^{-1}$, we obtain $L_D \sim 5$ cm. The timescale for so-called rubble mantle growth (neglecting cohesion) is (Jewitt 2002)

$$\tau_M \sim \frac{\rho_n L_D}{\dot{m} f_M} \tag{8}$$

in which ρ_n is the density of the nucleus, $f_M(r_n, R)$ is the fraction of the solid matter in the nucleus too large to be ejected by gas drag and $\dot{m}(R)$ is the specific mass sublimation rate. This timescale is only $\sim 10^3$ yr at 5 AU, falling to 1 yr at 3 AU for a water ice composition (Figure 5). The essential points are that rubble mantles can be very thin and should readily form as by-products of cometary activity on timescales that are short compared to τ_{JFC}. A feature of the rubble mantle model is that such structures should be unstable to ejection on comets whose perihelia diffuse inwards, since rising temperatures and gas pressures can easily overcome the local gravitational force. Cohesion between mantle grains is needed to convey long-term mantle stability to such objects (Kührt and Keller 1994).

A second kind of mantle is postulated for the cometary nuclei. The so-called irradiation mantle consists of material that has been chemically transformed and devolatilized by prolonged exposure to energetic photons and particles. Cosmic rays with Mev and higher energies penetrate to column densities $\sim 10^3$ kg m^{-2}, corresponding to depths $\sim$1 meter in material of density 10^3 kg m^{-3}. The timescales for complete processing of this surface layer are of order $10^{8\pm1}$ yr (Shul'man 1972). This is short compared to the storage times for bodies in the Oort Cloud and Kuiper Belt and the upper layers of residents of these populations are likely to be significantly processed down to meter depths. Optical photons, on the other hand, probe a surface layer only a few microns thick. The timescale for processing this visible layer is probably short, but the timescales for building a rubble mantle are even shorter. Thus, we expect that bodies with perihelia beyond the water sublimation zone (KBOs, Centaurs) might retain irradiation mantles but that these will have been ejected or buried on the nuclei of near-Earth comets. One observation consistent with this is the lack of ultrared

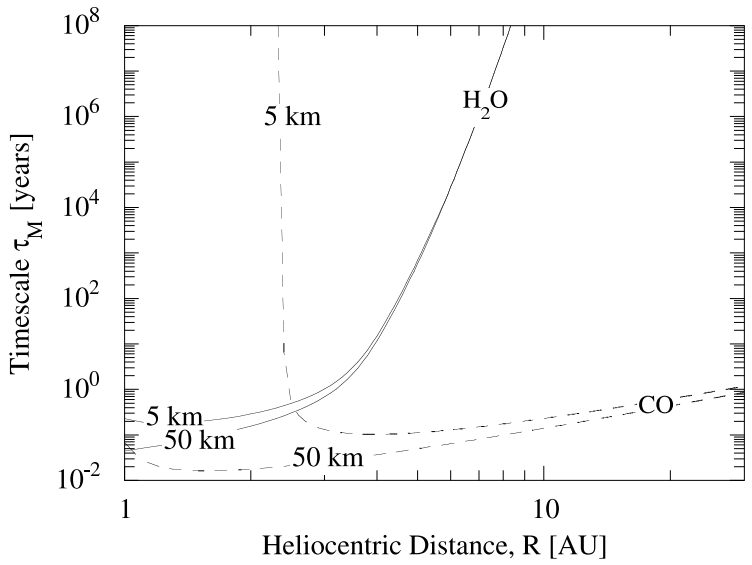

Fig. 5. Timescale for the growth of a rubble mantle in model nuclei of radii 5 km and 50 km, in response to sublimation of H_2O and CO ices and computed from Eq. (8). The orbits are assumed to be circular. Adoption of more realistic eccentric orbits would increase the mantling time relative to the plotted curves, but mantling is always rapid at small R. From Jewitt (2002).

matter, of the type seen on the surfaces of half the KBOs and Centaurs, on the nuclei of JFCs (Jewitt 2002; see section 4.7).

Irradiation breaks the chemical bonds of common molecules. In the process hydrogen, because of its small size, is able to escape from the irradiated layers of the nucleus into space. The irradiation mantle is thus composed of material in which the C/H and O/H ratios are high. The high carbon fraction may be responsible for the low albedos of cometary nuclei (Campins and Fernández 2002, Moroz et al. 2003). The low hydrogen fraction may explain why near infrared spectra of outer Solar system bodies, including KBOs, Centaurs, Jovian Trojans and cometary nuclei are mostly devoid of the absorption bands of common bonds (e.g. $C-H$, $O-H$, $N-H$).

4.2 Thermal Devolatilization

The timescale for the loss of volatiles from a mantled ice nucleus is

$$\tau_{dv} \sim \frac{\rho_n r_n}{f\overline{\dot{m}}} \tag{9}$$

where $\overline{\dot{m}}$ [kg m^{-2} s^{-1}] is the specific mass loss rate averaged around the cometary orbit, ρ_n is the density and f is the so-called 'mantle fraction', the

fraction of the surface from which sublimation proceeds. The specific mass loss rate can be estimated from equilibrium sublimation of H_2O ice to be about $\dot{m} \sim 10^{-4}$ kg m^{-2} s^{-1} at $R = 1$ AU, varying roughly as R^{-2} for $R \leq 2$ AU and faster than R^{-2} at greater distances (Figure 6). For non-zero orbital eccentricities, the sublimation rate at a given semimajor axis is higher than for the circular orbit case because of enhanced sublimation near perihelion. This effect is large only for orbital semi-major axes greater than about 3 AU, which is the critical distance beyond which sublimation consumes a negligible fraction of the absorbed Solar energy. This is shown in Figure 6, in which we plot the orbitally-averaged water ice sublimation rate as a function of semimajor axis and eccentricity. For the canonical JFC orbit with $a = 3.5$ AU and $e = 0.5$, we estimate $\overline{\dot{m}} = 10^{-5}$ kg m^{-2} s^{-1} (Figure 6). With $\rho_n = 500$ kg m^{-3} and $f = 0.01$ (A'Hearn et al. 1995), we find

$$\tau_{dv} \sim 2 \times 10^5 r_n \text{ yr} \tag{10}$$

with r_n again expressed in km and τ_{dv} in years. The effect of non-zero eccentricity is small for comets whose semi-major axis is less than the critical distance for strong sublimation of water ice ($R \leq 3$ AU, Figure 6). Thus, JFC lifetime estimates are much less affected than HFCs and LPCs, the latter of which sublimate only for a limited period near perihelion.

The lifetimes of kilometer scale nuclei against sublimation (given by Eq. 10) are comparable to the dynamical lifetime. Note that $\tau_{dv} < \tau_{JFC}$ for $r_n < 1$ km (Figure 2, point B). This means that the subkilometer comets should lose their volatiles on timescales short compared to their dynamical lifetimes, leaving behind a population of 'dead comets'. Note also that $\tau_{dv} < \tau_c$ for $r_n > 1$ km (Figure 2, point C), meaning that for almost all observed comets the volatiles are lost from the surface before the thermal conduction wave has reached the core. This inequality suggests another end state as 'dormant comets' (Hartmann et al. 1987, Kresak 1987), having devolatilized, inactive surface regions shrouding an ice packed core.

4.3 Size Evolution

Mass loss should modify the size distribution of the comets by selectively depleting the smallest objects (Eq. 10). The size distribution of the parent KBOs has been measured, albeit only for large objects, from the slope of the cumulative luminosity function (i.e. the cumulative number of objects per square degree of sky brighter than a given magnitude). Different researchers have converged on a power-law type distribution in which the number of objects with radius between r and $r + dr$ is

$$n(r)dr = \Gamma r^{-q} dr \tag{11}$$

with Γ and q constants of the distribution. The best fit value for KBOs is $q = 4.0^{+0.6}_{-0.5}$ (Trujillo et al. 2001). In such a distribution, the mass is spread uniformly in equal logarithmic intervals of radius while the cross-section is dominated by

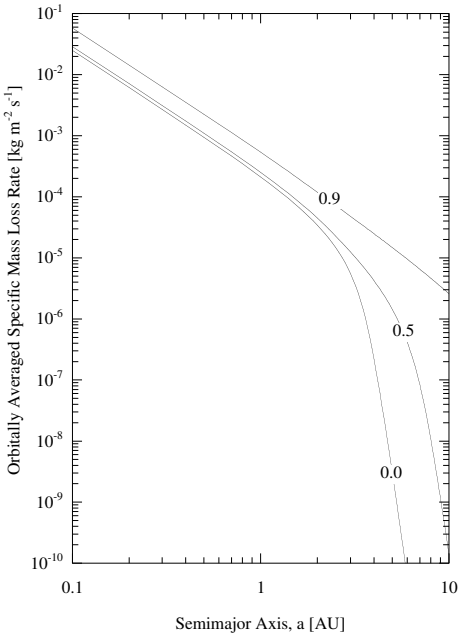

Fig. 6. Orbitally averaged specific mass loss rate for sublimating water ice as a function of the semimajor axis and eccentricity. The instantaneous mass loss rate was computed from the energy balance equation and integrated around the orbit using Kepler's equation. A low (0.04) albedo surface was assumed and thermal conduction was neglected. Curves are labelled by the orbital eccentricity.

the smallest objects in the distribution. The Centaurs are, by and large, less well observed than the KBOs. The available data are compatible with $q = 4.0 \pm 0.5$ (Sheppard et al. 2000). This is identical to the value in the Kuiper Belt, as expected if the latter is the source of the Centaurs.

The size distribution of the cometary nuclei is poorly determined by comparison. Fernández et al. (1999) used spatially resolved photometry of comets to find $q = 3.6 \pm^{0.3}_{0.2}$ while the same technique used independently by Weissman and Lowry (2003) gave $q = 2.6 \ \pm 0.03$ and Lamy et al. (2004) found $q = 2.6 \pm 0.2$ to $q = 2.9 \pm 0.3$. The results are inconsistent at the 5 σ level of significance. To understand this, it is important to remember that the cometary nuclei are in general observed in the presence of coma. Coma contamination of the nucleus photometric signal may confuse the results obtained by one or more of these groups. Furthermore, the short-period comets which form their samples have been discovered by a variety of techniques, each of which must impress onto the sample its own distinctive discovery bias. Naively, this bias is expected to favor cometary nuclei with large active areas because these objects will be bright and

therefore more easily detected. Over-representation of the bright comets will lead to a measured size distribution that is flatter than the intrinsic distribution.

What should we expect? Sublimation lifetimes of otherwise equal bodies vary in proportion to the radius (Eq. 10). Thus, in steady state, we expect that a source population described by r^{-q} should be flattened by sublimation to $r^{-(q-1)}$, as a result of the more rapid loss of the smaller objects. From $q = 4$ in the Kuiper Belt, we expect to find $q = 3$ among the JFCs, which is in between the measured values.

Comets with $r_n \leq 700$ m have $\tau_c \leq \tau_{dv}$ (Eqs. 7 and 10 and Point C in Figure 2). In such objects, the thermal conduction wave reaches ices still frozen in the core. The resulting gas pressure produced by sublimation in the core is likely to explosively disrupt the nucleus. This provides one possible explanation for the often reported depletion of very small comets relative to extrapolations of the power law size distribution as determined at kilometer and larger nucleus scales. The very short timescale for rotational spin-up of subkilometer nuclei (Figure 2: Jewitt 1999) provides an even more compelling mechanism for their destruction by rotational bursting.

It should be noted that the sizes of the measured KBOs and comets are quite different. Most KBOs have $r_n \geq 50$ km while most studied comets have $r_n \leq 5$ km. Size dependent, rather than evolutionary, effects might be present. It will be important to extend the KBO size distribution to typical cometary nucleus scales.

In summary, the size distributions of the KBOs and Centaurs appear identical, within the uncertainties, and consistent with the link between KBOs and Centaurs. Measurements of the size distributions of the cometary nuclei have been attempted, but the reported values are discordant and are, in any case, afflicted by discovery and coma contamination biases that are poorly understood.

4.4 Shape Evolution

The shapes of cometary nuclei can be estimated from their rotational lightcurves (strictly, the lightcurves give only the projection of the shape in the plane of the sky). If the nuclei are collisionally produced fragments, then it seems reasonable that their shapes should be distributed like those of impact fragments produced in the laboratory by impact experiments. The comparison is made in Figure 7 where we show the photometric ranges of well-measured nuclei with the range distribution of impact fragments measured in the laboratory by Catullo et al. (1984).

The distributions are clearly different, with the comets showing a larger fraction of highly elongated shapes than the impact fragments. The well-measured cometary nuclei are also elongated, on average, compared to main-belt asteroids of comparable size (Jewitt et al, 2003). This can be naturally explained as a simple consequence of anisotropic mass loss from the comets, which should act to modify the overall shape on a timescale comparable to τ_{dv}. Anisotropic mass loss may also provide a mechanism for splitting on this timescale (Hartmann and Tholen 1990). Note that most of the axis ratios reported in Table 1 of Lamy et

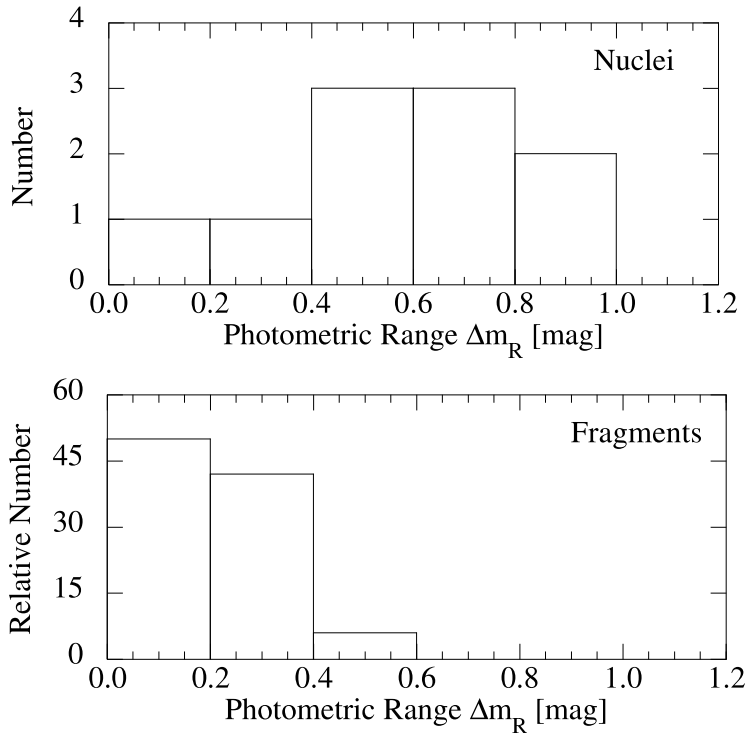

Fig. 7. Apparent axis ratios of cometary nuclei (from Jewitt et al. 2003) with published rotational lightcurves compared with impact produced rock fragments (from Catullo et al. 1984).

al (2004) are smaller than those in Figure 7. The difference might occur because the Lamy et al. data are lower limits obtained from sparsely sampled photometric series whereas the projected axis ratios in Figure 7 were all determined from well-measured lightcurves.

4.5 Spin Evolution

Non-central mass loss from the comets generates torques that can both change the spin period and drive the nucleus into an excited rotational state (i.e. a state other than principal axis rotation around the short axis). The relevant excitation timescale is

$$\tau_{ex} \sim \left[\frac{\omega \rho r_n^4}{V_{th} k_T \dot{M}} \right] \tag{12}$$

where $\dot{M}$ [kg s^{-1}] is the net mass loss rate from all active areas (for a spherical nucleus $\dot{M} = 4\pi r_n^2 f \dot{m}$), k_T is the dimensionless moment arm for the torque (k_T = 0 for radial ejection and k_T = 1 for tangential mass loss), and V_{th} is the

mass-weighted outflow speed (c.f. Samarasinha et al. 1986; Jewitt 1991). The dimensionless moment arm has been estimated analytically from a block model of the nucleus as $k_T \sim 0.05$ (Jewitt 1999) and from numerical simulations as $0.01 \leq k_T \leq 0.04$ (Gutiérrez et al. 2003). For plausible estimates of the parameters we find $\tau_{ex} < \tau_{JFC}$ (Figure 2), meaning that outgassing torques can drive comets towards rotational instability, perhaps providing one mechanism for destruction of the nucleus (Figure 2 and Jewitt 1999).

Excited rotational motions create periodic internal stresses that lead to minute (but, over long periods, significant) frictional dissipation of energy. Relaxation into the minimum rotational energy (maximum moment of inertia) state occurs on the timescale (Burns and Safranov 1973)

$$\tau_{damp} \sim \frac{\mu Q}{\rho K_3^2 r_n^2 \omega^3} \tag{13}$$

Here, μ $[Nm^{-2}]$ is the rigidity, Q is the quality factor (fractional loss of energy per cycle), K_3 is a shape-dependent numerical factor and r_n [m] is the mean radius. The damping parameters appropriate to cometary nuclei are not well known. We follow Harris (1994) and take $\mu Q = 5 \times 10^{11}$ $[N\ m^{-2}]$ and $K_3^2 \sim 0.03$ (based on data for Phobos). Substituting $\rho = 500\ kg\ m^{-3}$ we obtain

$$\tau_{damp} \sim 1.0 \times 10^5 \left(\frac{P^3}{r_n^2} \right) \tag{14}$$

for the damping time in years, with P in hours and r_n in km (Figure 2). A 2 km radius nucleus created collisionally in the Kuiper Belt with an initial spin period of 6 hr, for example, could occupy a rotationally excited state (Giblin and Farinella 1997) for only $\sim 10^7$ yr before damping away. This is comparable to the median transport time from the Kuiper Belt to the inner solar system. Comets much smaller than $\sim$2 km, and those with spin periods much longer than 6 hr, might retain excited rotational states produced collisionally in the Kuiper Belt, although we do not expect this to be the general case because the injection of a nucleus into a Neptune crossing orbit may occur long after its collisional production.

Nucleus excitation is much more likely to be actively produced once comets begin to outgas inside the orbit of Jupiter. The timescales for excitation (Eq. (12)) and damping (Eq. 13) of the spin are equal at the critical size

$$r_n = \left(\frac{4\pi \mu Q V_{th} k_T f \dot{m}}{\rho^2 K_3^2 \omega^4} \right)^{1/4} \tag{15}$$

which, with $\dot{m} = 10^{-5}$ kg $m^{-2} s^{-1}$, $V_{th} = 10^3$ m s^{-1}, $\rho = 500$ kg m^{-3}, $f = 0.01$, $P = 6$ hr and other parameters as given earlier yields $r_n \sim 20$ km (Figure 2, point D). Since most known cometary nuclei are smaller than this critical size, we conclude that most are potentially in rotationally excited states. Numerical simulations show that Eq. (12), while providing a good estimate of the timescale for spin-up, may give only a lower limit to the timescale for driving a nucleus into excited rotational states (Gutiérrez et al. 2003). Thus it is possible that Eq.

(15) over estimates the critical radius.

Observational evidence for precession of the nuclei is limited, both because measurements are complicated by the effects of near-nucleus coma and because few attempts have been made to secure adequate temporal coverage. The best case is for the nucleus of 1P/Halley (Samarasinha and A'Hearn 1991) while, more recently, 2P/Encke has shown indications of a time-varying lightcurve that might indicate nucleus precession (Fernández et al. 2000). Spin-up might be expected to lead to rapid rotation among the comet nuclei, especially at small sizes. A few nuclei (P/Schwassmann-Wachmann 2, Luu and Jewitt 1992b) are indeed rotating close to the centripetal limit for densities $\rho \sim 500$ kg m^{-3}. Less direct evidence for rotational destruction of small nuclei might be evident in the depletion of these objects relative to power law extrapolations from larger sizes.

4.6 Active Area Evolution

The active areas and the mantle should evolve in parallel. The lifetime of an active area can be estimated as follows. In the limiting case in which all the incident Solar energy is used to sublimate ice, the subsolar specific mass loss rate is given by

$$\dot{m} = \frac{S_\odot}{LR^2} \tag{16}$$

in which $S_\odot = 1360$ W m^{-2} is the Solar constant, R [AU] is the heliocentric distance and L is the latent heat of sublimation at the (sublimation depressed) temperature of the surface ice. (We consider the limiting case only because it gives a convenient analytic expression for $\dot{m}$). The corresponding rate of recession of the sublimating surface is just

$$\dot{r} \sim \frac{\dot{m}}{\rho}. \tag{17}$$

An exposed plug of ice of area $\pi a^2 = 4\pi r_n^2 f$ would sublimate into the nucleus, creating a cavity or vent that deepens at rate $\dot{r}$. When the vent becomes too deep, self-shadowing by the walls will inhibit further sublimation. Accumulation of a blocky rubble mantle at the bottom of the vent will also suppress sublimation. We assume that this happens first when the vent reaches a critical depth $d \sim a$. The timescale for the vent to reach this depth is just $\tau_v \sim a/\dot{r}$. From Eq. (17) we obtain

$$\tau_v \sim \frac{2 f^{1/2} \rho R^2 L r_n}{S_\odot} \tag{18}$$

where ρ is the density of the solid ice. For H_2O ice ($L = 2{\times}10^6$ J kg^{-1}) with $\rho = 500$ kg m^{-3}, $f = 0.01$ and $R = 1$ AU, we obtain

$$\tau_v \sim 5\ r_n \text{ yr} \tag{19}$$

with r_n expressed in km and the lifetime is years of exposure to sunlight in a circular orbit at $R = 1$ AU. A 5 km radius nucleus would have $\tau_v \sim 25$ years. The vent lifetime on the nucleus of an equivalent comet moving in an eccentric orbit will be larger because the mean insolation and the mean mass loss rate are smaller. For example, a JFC with $a = 3.5$ AU, $q = 1.0$ AU would have a vent timescale longer than given by Eq. (19) by a factor of ∼10 to account for the greater mean distance from the sun. Still, the vent lifetimes are expected to be very short compared to the dynamical lifetime, τ_{JFC}, for comets on all but the most eccentric orbits. Observational constraints on JFC active area lifetimes are few: Sekanina (1990) concludes that changes in active areas should be evident on timescales comparable with the observing records of many comets, consistent with Eq. (19).

For a CO powered vent ($L = 2 \times 10^5$ J kg^{-1}) on a KBO at $R = 40$ AU, the timescale is still a short $\tau_v \sim 8 \times 10^2$ yr. Active areas on the same object moved to $R = 10$ AU would become self-shadowing in only ∼ 50 yr, a tiny fraction of the dynamical lifetime. We conclude that the KBOs and Centaurs may occasionally display spectacular CO powered comae from exposed vents (e.g. craters produced by impact), but that these are short-lived and should therefore be rare unless the vents are reactivated or replaced. Centaur 2060 Chiron exhibits brightness outbursts in the $8 \leq R \leq 19$ AU range with a timescale ∼ 10 to 20 yrs (Bus et al. 2000). It is not unreasonable to suppose that this activity is modulated by the evolution of CO powered vents. Centaur C/2001 T4 likewise displays a prominent, variable coma at $R \sim 8.5$ AU (see Figure 3 and Bauer et al. 2003). In the comets (and, to a lesser extent the Centaurs) reactivation and the formation of new active areas may be driven by the progressively rising temperatures leading to increasing gas pressures that can destabilize the mantle (Brin and Mendis 1979, Rickman et al. 1990). In the rather stable orbits of the Kuiper Belt, reactivation can be caused by impacts that disrupt the mantle.

4.7 Colors and Albedos

Figure 8 shows distributions of the optical colors of different types of small bodies (Table 2 summarizes the data). The KBOs show a wide range of colors from nearly neutral ($S' > 0$ %/1000Å) to very red ($S' \sim 50$%/1000 Å) with a median value $S' = 25$ %/1000Å. Here, the slope, S', is measured in the best-observed $V - R$ region of the spectrum (i.e. 5500Å to 6500Å wavelength). The similarity between the wide spread of colors on the KBOs and on the Centaurs (here taken from Bauer et al. 2003b) shows that mantling on the Centaurs is relatively minor, even though these bodies may sometimes be active (Figure 8). Instead, a dramatic change in the color distribution appears only once the bodies have perihelia inside Jupiter's orbit and can begin to sublimate water ice. The comets show a smaller range of S' and, specifically, are deficient in the ultra-red material with $S' > 25$ %/1000Å (Jewitt 2002, see also Hainaut and Delsante 2002). This may be a result of mantling of the cometary nuclei driven by sublimation in response to rising temperatures as they approach the sun. Objects that are likely, on dynamical grounds, to be dead comets show a color

distribution that is formally indistinguishable from that of the nuclei of active comets, suggesting that the mantles on these bodies are stable over long periods (and may, indeed, be responsible for the deaths of the comets; Rickman et al. 1990).

Table 2. Mean Reflectivity Gradients and Color Indices

Object	S'	V-R	N	Reference
KBOs	23 ± 2	0.61 ± 0.01	28	Jewitt and Luu 2001
Centaurs	22 ± 4	0.58 ± 0.01	24	Bauer et al. 2003b
Nuclei	8 ± 3	0.45 ± 0.02	12	Jewitt 2002
Dead Comets	7 ± 2	0.44 ± 0.02	12	Jewitt 2002
D-Types	8.8 ± 0.5	0.45 ± 0.01	19	Fitzsimmons et al 1994
Trojans	10 ± 1	0.46 ± 0.01	32	Jewitt and Luu 1990

A similar conclusion can be drawn from Figure 9, in which we show available measurements of the colors and albedos of the small-body populations. It is evident that the cometary nuclei occupy a restricted region of the color-albedo plane near $p_R \sim 0.04$, $S' \sim 10$ %/1000Å while the Centaurs are much more widely dispersed. The few measured nuclei fall near the region occupied by the D-type asteroids and the similarity with the Trojans is impressive (Jewitt and Luu 1990). The corresponding data for KBOs, although few in number, already show wide separation in the color-albedo plane and are very different from any cometary nucleus yet measured. Observationally, we can already state with confidence that the albedos and colors of the cometary nuclei occupy a smaller range than is found in the Centaurs or KBOs. The implication is that surface materials that are common in the middle and outer Solar system, including frosts and the ultrared material, have been ejected or buried (Jewitt 2002) or are thermodynamically unstable (Moroz et al. 2003) on the JFCs. The significance of this result is that spacecraft launched to investigate the nuclei of JFCs may fail to sample the primitive materials present on the surfaces of their more distant progenitors.

5 Cometary End States

5.1 Dead and Dormant Comets

Dormant comets lack near-surface volatiles but may possess ice-rich interiors while dead comets are completely devolatilised. Identifying such objects from their physical properties is not easy, since the nuclei possess a wide range of optical properties that overlaps those of some classes of asteroids. The orbital properties provide a separate clue: dead and dormant comets are likely to possess comet-like Tisserand invariants, $T_J \leq 3$. Objects selected on this basis indeed possess low, comet-like geometric albedos, $p_R \sim 0.04$ (see Figure 10), quite distinct from the $T_J > 3$ asteroids. This finding has been used to infer that about 10% of the near-Earth objects (NEOs) might be dead comets (Fernández et al.

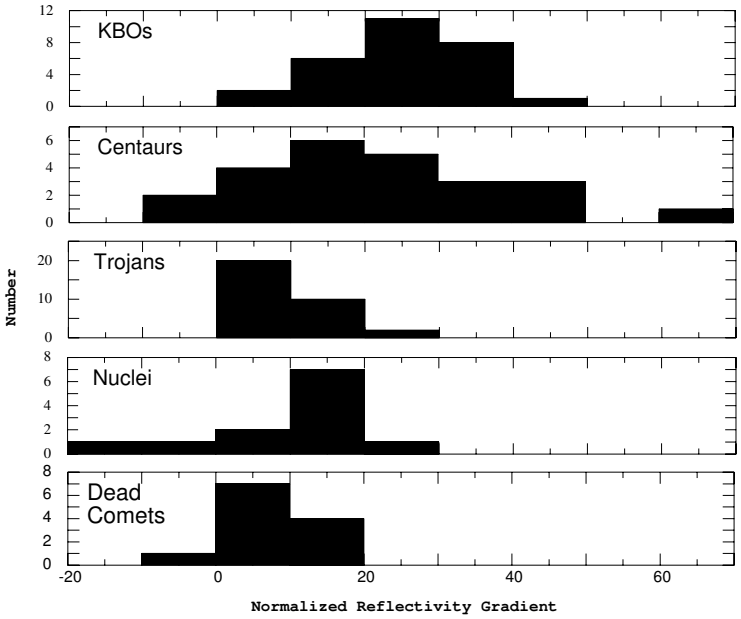

Fig. 8. Histograms of normalized optical reflectivity gradients (%/1000 Å) for objects in the major categories of this review. Plotted are: KBOs, nuclei and dead comets (Jewitt 2002), Centaurs (Bauer et al. 2003b) and Jovian Trojans (Jewitt and Luu 1990). The ultrared matter, with reflectivity gradient $\geq$ 25 %/1000 Å, is present only in the Kuiper Belt and on the Centaurs.

2001). Dynamical models of the Near Earth population allow a similar ($\sim$ 6 %) fraction of dead comets (Bottke et al. 2002). However, the latter models are incomplete in that they neglect non-gravitational forces and/or perturbations from the terrestrial planets. Orbits decoupled from Jupiter, like that of comet P/Encke ($T_J = 3.03$), cannot be reproduced without including these effects. Calculations in which these forces are included suggest that the dead JFC fraction of the near Earth population is $\leq$ 20% (Fernández et al. 2002) to 50% (Harris and Bailey 1998). The results remain uncertain, in part, because the form and time-dependence of the non-gravitational acceleration remain poorly known. Furthermore, the magnitude of the non-gravitational acceleration, all else being equal, varies inversely with the nucleus radius so that size-dependent effects in the dynamics should be expected. Realistic modelling of the orbital evolution of

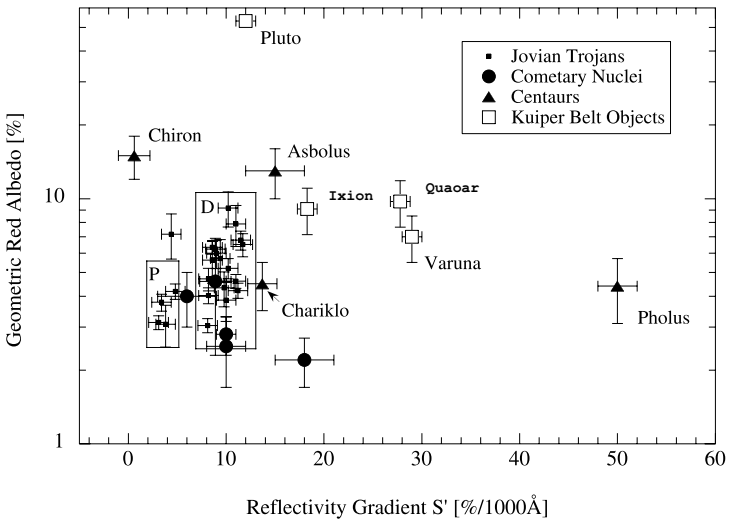

Fig. 9. Plot of normalized reflectivity gradient vs. geometric albedo for Jovian Trojan asteroids, cometary nuclei, Centaurs and two Kuiper Belt Objects (see legend for a key to the symbols). Boxes mark the approximate regions of the P and D asteroid spectral classes according to Dahlgren and Lagerkvist 1995. The Trojan data are compiled from Jewitt and Luu (1990) and Tedesco et al. (2002), Centaur data from Jewitt and Luu (2002), Hainaut and Delsanti (2002) and Campins and Fernández (2002), and the KBO data are Pluto (Tholen and Buie 1997), 20000 Varuna (Jewitt et al. 2001, Hainaut and Delsanti 2002), 28978 Ixion and 50000 Quaoar (Marchi et al. 2003 and Bertoldi et al 2002).

outgassing comets is potentially very complicated and deserves more attention than it has yet received.

Rubble mantles, unless held together by granular cohesion, are susceptible to ejection in response to decrease of the perihelion (Rickman et al. 1990). The transition to the asteroidal state may include a protracted period of intermittent cometary activity as the mantle cracks and reseals. Several examples of comets in which the activity is extremely weak (e.g. 49P/Arend-Rigaux, 28P/Neujmin 1) or may even flicker on and off are known (Kresak 1987).

Several comets and likely comets are known to follow asteroid-like orbits (see Table 3 and Weissman et al. 2002 for more detailed descriptions). The most famous example is comet 2P/Encke, which is a bona-fide comet that has decoupled from Jupiter's control ($T_J = 3.03$). Comet 107P/Wilson-Harrington (also known as asteroid 1949 W1) displayed a diffuse trail at discovery in 1949 (Figure 11) but has appeared asteroidal ever since (Fernández et al. 1997). The object 3200 Phaethon appears dynamically associated with the Geminid meteor stream, yet has shown no evidence for recent outgassing and occupies a thoroughly un-comet-

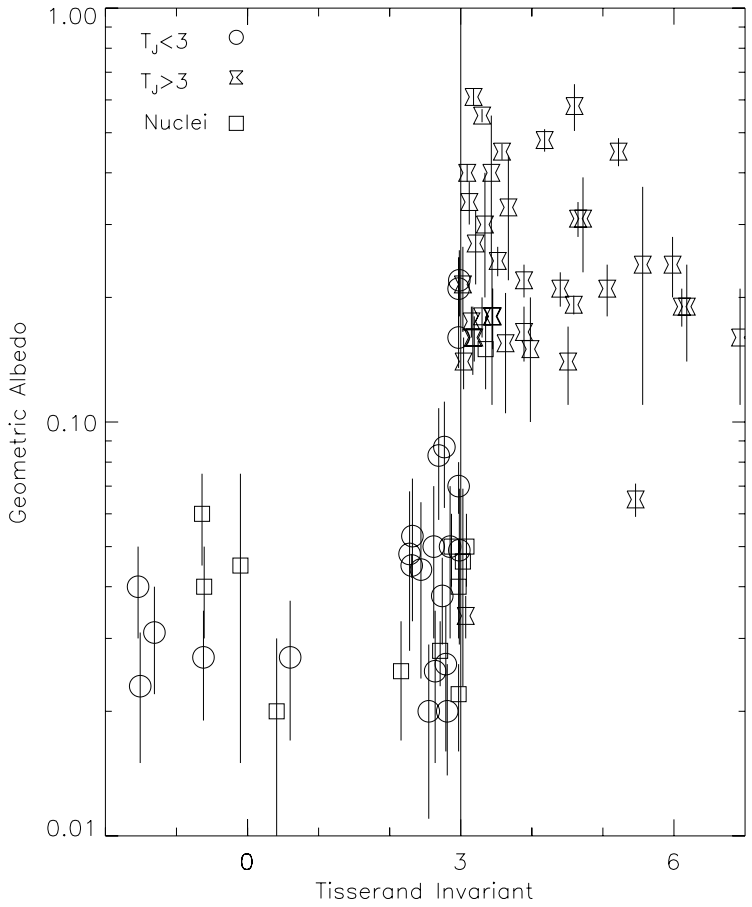

Fig. 10. Plot of red (0.65 μm) geometric albedo, p, versus Tisserand parameter, T_J, for small Solar system bodies including dynamically asteroidal Near Earth Objects ($T_J > 3$), unresolved objects likely to be inactive comets on dynamical grounds ($T_J \leq 3$) and the nuclei of active comets. From Fernández, Jewitt and Sheppard 2003.

like orbit. Lastly, asteroid 7968 was found to show a dust trail in images taken in 1996, leading to this object being cross-identified with comet 133P/Elst-Pizzaro. The confinement of the dust to the vicinity of the orbit plane shows that the observed particles experience a small ratio of forces due to radiation pressure relative to Solar gravitational attraction. This, in turn, suggests that the particles are large, probably at least 10 - 20 μm in size. The existence of a dust trail from this object is particularly puzzling, since it is dynamically a main-belt asteroid with orbital elements consistent with those of the Themis family (Table 3). It has been suggested that the appearance of outgassing activity might have been created by a recent collision with a smaller asteroid (Toth 2000), but this explanation seems unlikely given the reappearance of the trail in Mauna Kea data

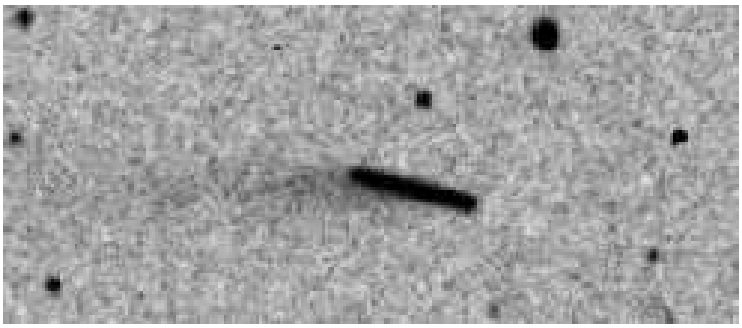

Fig. 11. Trailed (unguided) image of asteroid-comet transition object 107P/1949 W1 (Wilson-Harrington) taken UT 1949 November 19. The trailed image of the central nucleus is about 1 arcmin. in length in this 720 sec. integration. North is at the top, East to the left, and the tail extends towards the east (antisolar) direction). The comet was 0.2 AU from Earth and 1.1 AU from the Sun. Palomar sky image from Fernández et al. (1997).

in 2002, 6 years after the initial detection (Hsieh et al. (2003), see Figure 12). Either 133P/Elst-Pizzaro is an asteroid somehow triggered to lose mass or it is a comet somehow driven into an asteroid-like orbit. The aphelion of 133P/Elst-Pizzaro at 3.80 AU is far from Jupiter's orbit. Non-gravitational accelerations from outgassing might produce this type of decoupling from Jupiter but with very low efficiency (Fernández, Gallardo and Brunini 2002).

Table 3. Comets and Likely Comets in Asteroid-Like Orbits

Object	Perihelion [AU]	Semimajor Axis [AU]	Eccentricity	Inclination [deg]	T_J
2P/Encke	0.34	2.22	0.85	11.8	3.03
3200 Phaethon	0.14	1.40	0.89	22.1	4.51
107P/Wilson-Harrington	1.00	2.64	0.62	2.8	3.08
7968 133P/Elst-Pizarro	2.63	3.25	0.17	1.4	3.18

A number of objects in comet-like ($T_J \leq 3$) orbits possess no resolvable coma or tail and must be physically classified as asteroidal. A fraction of these could be dead (or dormant) comets. Based on their lifetimes, the ratio of the numbers of dead, N_d, to active, N_a, comets should be

$$\frac{N_d}{N_a} \sim \frac{\tau_{JFC}}{\tau_{dv}} \sim \frac{2}{r_n}. \tag{20}$$

The number of NEOs larger than $\sim$ 1 km in size is $\sim$1000 (Rabinowitz et al. 2000, Bottke et al. 2002). If $\sim$ 10 % of these are dead or dormant comets (Fernández et al. 2001, Bottke et al. 2002), then the number of such objects

Table 4. Sample Asteroids in Comet-Like Orbits

Object	Perihelion [AU]	Semimajor Axis [AU]	Eccentricity	Inclination [deg]	T_J
5335 Damocles	1.57	11.82	0.87	62.0	1.15
15504 1998 RG33	2.15	9.43	0.77	34.9	1.95
20461 1999 LD31	2.39	24.43	0.90	160.2	-1.54
3552 Don Quixote	1.21	4.23	0.71	30.8	2.32
1997 SE5	1.24	3.73	0.67	2.6	2.66
1982 YA	1.12	3.66	0.70	35.3	2.40

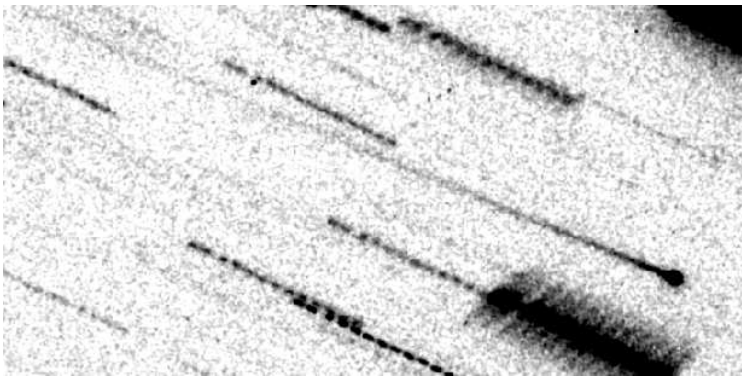

Fig. 12. 133P/(7968) Elst-Pizarro in a 3900 sec., R-band composite image taken on UT 2002 September 07 at the University of Hawaii 2.2-m telescope. Short trails are background stars and galaxies. The nucleus of 133P has been placed at the lower right. Image is 180 arcsec wide, with North at the bottom and East to the right. The heliocentric and geocentric distances were 2.88 AU and 1.96 AU, respectively, and the phase angle was 9.9 deg. A dust trail is visible across the full width of the image in the raw data. Image by Henry Hsieh and the author.

must be ∼100. For comparison, about 200 JFCs are known while the true (bias corrected) population may number in the thousands (Fernández et al. 1999). Empirically, then, $N_d/N_a < 0.5$, whereas Equation (20) gives $N_d/N_a \sim 2$ for $r_n = 1$ km.

Models of the orbital evolution of JFCs permit an independent estimate of N_d/N_a. The models show that the mean inclination increases with residence time in the inner Solar system (Levison and Duncan 1994, 1997). To bring the model and observed inclination distributions of the JFCs into agreement, these authors found it necessary to assume that the JFCs are active for between 3,000 and 30,000 yrs (with a best estimated value of about 12,000 yrs) after their perihelion first reaches $q \leq 2.5$ AU. The corresponding ratio of dead to active JFCs is $2 \leq N_d/N_a \leq 6.7$, with a best estimate of $N_d/N_a = 3.5$ (Levison and Duncan 1997). Whether or not the difference between the measured and model values of N_d/N_a is significant is unclear.

5.2 Tidal Breakup

A small number of comets have been observed to break up in response to gravitational stresses induced by close proximity to the Sun (e.g. the Kreutz sungrazer group) or a planet (commonly Jupiter, as with P/Brooks 2 and D/Shoemaker-Levy 9). The properties of the 'string of pearls' comet chain produced from D/Shoemaker-Levy 9 are well explained by a disrupted, gravitationally sheared aggregate body of negligible tensile strength and density $\rho_n \sim 500$ kg m^{-3} (Asphaug and Benz 1996).

Some 4% of the Centaurs pass within the Roche radius of a gas giant planet during their lifetimes (Levison and Duncan 1997). If, like D/Shoemaker-Levy 9 (which had 26 fragments), each object splits into a few dozen pieces, then the number of secondary fragments could rival or even exceed the number of primary comets from the Kuiper Belt. This would have significant implications for the flux, size, mass and rotation distributions of the comets. For example, tidal breakup could reduce the number of small KBOs needed to supply the JFC flux (c.f. Bernstein et al. 2003). Most split comet fragments would quickly mix with the primary unsplit population: dynamical memory of the splitting is quickly lost (Pittich and Rickman 1994).

5.3 Non-Tidal Breakup

Most splitting events occur without obvious provocation and their cause is unknown (Sekanina 1997). Statistically, the nuclei of JFCs split at a rate $\tau_{split}^{-1} \sim 10^{-2}\ \ yr^{-1}$ per nucleus (Chen and Jewitt 1994, c.f. Weissman 1980). With dynamical lifetimes of a few $\times 10^5$ yr, each nucleus should split thousands of times. The rate for the observed long period comets is less well constrained but probably of the same order. The effect of repeated splittings on the mass of the primary nucleus depends on δ, the mass-weighted fragment to primary nucleus mass ratio. If splitting is a continuous random process, the fraction of the mass remaining in the primary after time, t, is just

$$\frac{m(t)}{m(0)} \sim (1-\delta)^{t/\tau_{split}}. \tag{21}$$

Setting $t = \tau_{dv}$ as an upper limit, we find $m(\tau_{dv})/m(0) << 1$ for $\delta >> 10^{-3}$. Observationally, the situation is unclear. Most fragments of the Kreutz sungrazing comets have characteristic sizes of ∼10 m, corresponding to $\delta \sim 10^{-6}$ for a kilometer sized parent (Sekanina 2002). If this is representative of splitting events as a whole, then it is unlikely that disintegration plays a major role in shaping the nuclei. However, if breakup is a continuous process that extends to much larger, but rarer fragment sizes, then the effect on the primary mass may still be significant.

The short timescales for spin excitation, τ_{ex} (see Figure 2), suggest that rotational bursting may play a role. The centripetal and gravitational accelerations on the equator of a spherical body of density ρ [kg m^{-3}] are equal at the critical rotational period

$$\tau_r = \left(\frac{3\pi}{G\rho}\right)^{1/2} \tag{22}$$

where $G = 6.6{\times}10^{-11}$ [N $kg^{-2}m^2$] is the gravitational constant. Strengthless objects rotating with periods $P_{rot} < \tau_r$ are susceptable to rotational bursting. For the more general case of an elongated body in minimum energy rotation (about the shortest axis), the critical period is

$$\tau_r \sim 3.3 \left(\frac{1000}{\rho}\right)^{1/2} f_r \ hr \tag{23}$$

where f_r is a numerical factor that depends on the axis ratio of the body (e.g. $f_r = 1$ for spheres, $f_r \sim 4/3$ for prolate bodies with axis ratio $a/b = 2$). Observationally, all but the smallest (strongest) asteroids, and all measured comets, have $P_{rot} \geq 2$ hours and consistent with $\rho \geq 500$ [kg m^{-3}] (Pravec et al. 2002). The most elongated comets may be rotating close to their corresponding centripetal limits (Jewitt and Meech 1988, chapter by Weissman et al.).

For example, the nucleus of C/1999 S4 (LINEAR) may have been as small as 100 meters in radius prior to break up into fragments at 0.85 AU (Weaver et al. 2001). Equation (12) gives $\tau_{ex} \sim 10$ days for such a small object when close to the sun. The nucleus could have been driven to rotational bursting during the time taken to free fall towards the sun. Split fragments themselves would be subject to rapid spin-up, leading to a cascade of rotationally bursting fragments.

5.4 Disintegration

Except for the sungrazing comets observed by SOHO, only a few well-documented examples of complete cometary disintegration are known (see chapter by Boehnhardt). This does not mean that complete disintegration is rare, because the probability that a brief, one-time event might be observed by chance is presumably very small. The causes of disintegration are not known.

Samarasinha (2001) suggested a model for the nucleus of C/1999 S4 (LINEAR), namely that fragmentation was due to the build up of gas pressure inside a loosely agglomerated nucleus having substantial internal void space. High pressures have been observed in association with the heating of amorphous ice samples in which clathrate formation may also play a role (Blake et al. 1991). This "bomb model" model predicts that small nuclei (e.g. SOHO comets) should detonate more readily than large ones, since the gravitational binding energy grows as r_n^5 while the gas pressure is independent of nucleus size. The real unknown in this model is the permeability to gas: if the gas can leak out the pressure may never grow large enough to burst the nucleus.

Rotational spin-up (Figure 2 and Eq. 12) might also be implicated in cometary disintegration. An elongated nucleus in simple rotation driven to the centripetal limit might be expected to lose mass only from its tips. The same nucleus in an excited rotational state might be pushed to disintegrate by rotational instabilities, particularly if the nearly strengthless internal constitution witnessed

in D/Shoemaker-Levy 9 is typical. Rotational ejection could also expose previously shadowed volatiles, initiating a sudden burst of outgassing and perhaps precipitating global instability of the nucleus.

Why some nuclei disintegrate while others split and others remain coherent is a mystery. Neither do we know if splitting and disintegration occur with uniform probability across all comets, or whether some comets are "born tough" and resist splitting and disintegration until their eventual demise. In the latter case, the surviving comets might not be at all representative of the comets prior to their entry into the inner Solar system. This possibility has been suggested as an explanation of the presumed fading of long period comets (Levison et al 2002).

5.5 Debris Streams

Meteor streams represent the final products of cometary disintegration. The known streams are observationally preselected to intersect the orbit of the Earth and are biassed towards long-period and HFC cometary sources (the luminosity of a meteor of given mass varies with a high power of the relative velocity so that LPC and HFC sources produce brighter meteors than JFC or asteroidal orbits, all other things being equal). Counterparts of the meteor streams for comets whose orbits do not intersect that of Earth are found in cometary dust trails detected thermally (Sykes and Walker 1992) and optically (Ishiguro et al. 2003). Some parameters of the major streams and their likely parents are listed in Table 5.

Table 5. Major Meteor Streams

Quantity	Quadrantid	Perseid	Orionid	Geminid	Leonid
Parent Object	5496	109P	1P	3200	55P
Parent Type	Asteroid	HFC	HFC	Asteroid	HFC
Perihelion q [AU]	0.88	0.9595	0.5860	0.14	0.9764
Eccentricity e	0.64	0.9632	0.9671	0.89	0.9055
Inclination i [deg]	68.0	113.5	162.3	22.1	162.5
Semimajor axis a [AU]	2.44	26.1	17.8	1.27	10.33
Tisserand T_J	2.53	-0.28	-0.61	4.51	-0.64
Stream Mass, M_s [kg]	1.3×10^{12}	3.1×10^{14}	3.3×10^{13}	1.6×10^{13}	5.0×10^{12}
Meteor Density [kg m^{-3}]	1900±200	1300±200	–	2900±600	400±100
Parent radius [km]	1.8	10.5	5.0	2.6	1.8
Parent Mass, M_p [kg]	1.2×10^{13}	2.4×10^{15}	2.6×10^{14}	3.7×10^{13}	1.2×10^{13}
$M_s/(M_s + M_p)$	0.10	0.13	0.13	0.38	0.29

The wide range of Tisserand invariants in Table 5 shows the dynamical diversity of the sources of the major meteor streams. Some are clearly linked to still-active comets; others are associated with objects that appear asteroidal (Hughes and McBride 1989, Williams and Collander-Brown 1998). Source diversity is also indicated by the wide range of meteor densities listed in the Table.

The absolute values of density are limited in accuracy by the fragmentation models applied in the interpretation of meteor data, but the relative densities should be meaningful (Babadzhanov 2002, Rubio et al. 2002). For example, debris from the Leonid parent 55P/Tempel-Tuttle is much less dense (more porous?) than debris from Geminid parent 3200 Phaethon. The stream masses are estimated from the flux of meteors as a function of time and are thought to be accurate to within a factor ± 4, or so (Hughes and McBride 1989, Jenniskens and Betlem 2000). The Table shows that the ratio of the stream mass to the stream plus parent nucleus mass is $0.1 \leq M_s/(M_s + M_p) \leq 0.4$. What is behind this ratio?

Consider a model of a spherical nucleus shrinking at a constant rate and, for simplicity, neglect mantle formation. Assuming that mass is not lost from the stream on the sublimation timescale, the ratio of the mass of the stream, M_s, to the total mass of the parent and stream, $M_s + M_p$, is given by

$$\frac{M_s}{M_s + M_p} = f_s \left[\frac{r_0^3 - r^3(t)}{r_0^3} \right] \tag{24}$$

where r_0 is the initial nucleus radius and $r(t) = r_0 - \beta t$ (β is a constant equal to the sublimation distance per unit time) is the radius at time t ($t \leq r_0/\beta$). The quantity f_s is the fraction of the mass of the parent that is contained in refractory matter.

Averaged over the time interval $0 \leq t \leq r_0/\beta$, the value of Eq (24) is given by

$$\overline{\frac{M_s}{M_s + M_p}} = \frac{3}{4} f_s. \tag{25}$$

With $f_s = 1/2$, we have $\overline{M_s/(M_s + M_p)} = 3/8 \sim 0.4$ which is very close to the measured values (Table 5). The observations are therefore consistent with the simple model, provided the stream debris lifetimes are long compared to the source lifetimes.

The lifetimes of the streams are poorly determined. Estimates based on dynamical scattering of Perseids suggest lifetimes of 4×10^4 yr to 8×10^4 yr (Brown and Jones 1998). Independently, the mass loss rate from the Perseid parent 109P/Swift-Tuttle has been estimated at 5×10^{11} kg/orbit from submillimeter observations (Jewitt 1996b). To supply the 3.1×10^{14} kg in the stream would require about 600 orbits, corresponding to 8×10^4 yr, in good agreement with the dynamical lifetime estimates, above.

6 Summary

Substantial progress has been made in recent years towards exploring and understanding two major storage regions of the comets, the Oort Cloud and the Kuiper Belt. The latter, in particular, has been transformed from a conjecture into a dynamically rich and observationally accessible region of the Solar system, about which we learn more seemingly every month. On the other hand,

the processes of decay of the comets, and the relationships which exist between these objects and other small bodies in the Solar system remain subjects of considerable uncertainty. The latter have been the troublesome subjects of this chapter.

Observationally, there are at least two challenging problems. First, the physical properties of the all-important cometary nucleus are difficult to measure, because of coma contamination when near the sun and because of nucleus faintness when far from it. In order to study how the comets evolve and decay, reliable measurements of the nuclei are indispensable. We possess very few. Second, telescopic data in any case sample only the outermost, optically active surface layers. We can learn relatively little about fundamental aspects of the internal structure or composition by sampling only reflected sunlight.

In terms of dynamics, the comets occupy difficult territory in which forces due to mass loss may play an important long-term role. The nuclei are pushed by asymmetrical (sunward directed) ejection of matter. Their angular momenta are changed by outgassing torques and their very lifetimes as comets may be limited by the loss of mass due to sublimation, and by rupture due to centripetal effects. Purely dynamical models appear to have been pushed to their limits. The next step is to couple dynamical models with thermophysical models in order to more realistically account for the effects of outgassing forces on the comets.

In terms of their formation, the comets and the asteroids represent two ends of a continuum. The asteroids, at least those of the main-belt, mostly formed at temperatures too high for the inclusion of water as ice while the comets accreted water ice in abundance, we think. In between lies a large grey zone, in which the identity of the objects is indistinct, both observationally and compositionally. We have discussed some examples of mass-losing objects that are dynamically more like asteroids than comets (e.g. 133P/Elst-Pizarro). The Jovian Trojan "asteroids" appear optically indistinguishable from the nuclei of comets and they may also contain solid ice. Unfortunately, they are too cold to measurably sublimate, even if ice is present in the near surface regions. Some asteroids in the outer belt could also contain ice, but only if buried by thicker, thermally insulating mantles. Conversely, the comets may be less ice rich than originally supposed in Fred Whipple's classic description. While it is no surprise that sun-baked 2P/Encke has a large dust/gas production rate ratio $\sim$10 to $\sim$30 (Reach et al. 2000), even the comparatively fresh comet C/Hale-Bopp had dust/gas $\sim$6 to $\sim$10 (Grün et al. 2001). It is not clear that these ratios are representative of the bulk interior values, but still, the difference between the "icy comets" and the "rocky asteroids" seems astonishingly small.

In the end, what matters most is that we can relate the properties of the small bodies of the solar system back to the formation conditions, to learn something about the processes of accretion and planet growth. Observations and ideas explored here represent some of the first steps in this direction. We end with a list of key questions that should be answered in the coming years.

6.1 Some Key Questions

- Processes described here (core volatile sublimation, rotational bursting, complete devolatilization) suggest that the comet nucleus size distribution should be depleted at small sizes. What reliable observational evidence exists for this?
- What fraction of the Near Earth Objects are dead comets and how can they be reliably distinguished from asteroids?
- Are the Trojans of Jupiter essentially mantled comets with substantial interior bulk ice? How can this question be answered?
- What is the true Centaur population as a function of size? Initial estimates of 10^7 objects larger than 1km in radius need to be checked by deeper, more extensive survey observations of the whole ecliptic.
- Are there sources of Centaurs (and Jupiter family comets) in addition to those recognized in the Kuiper Belt? Are the Trojans of the four giant planets a significant source?
- What fraction of the Centaurs are fragments of precursor objects that were disrupted by passage through the Roche spheres of gas giant planets?
- Is there any firm evidence for outgassing in the KBOs?
- What is the physical basis of the "fading parameter" in Oort's model of the long-period comets? Is our understanding of the dynamics of the LPCs complete?

7 Acknowledgements

I thank Dale Cruikshank, Yan Fernández, Michel Festou, Jane Luu, Nalin Samarasinha, Scott Sheppard and the anonymous referee, Paul Weissman, for their comments on this manuscript. Support from NASA and NSF is gratefully acknowledged.

References

1. A'Hearn, M., Millis, R., Schleicher, D., Osip, D., and Birch, P. (1995). The ensemble properties of comets: Results from narrowband photometry of 85 comets, 1976-1992. Icarus, 118, 223-270.
2. Asphaug, E. and Benz, W. (1996). Size, Density, and Structure of Comet Shoemaker-Levy 9 Inferred from the Physics of Tidal Breakup. Icarus, 121, 225-248.
3. Babadzhanov, P. (2002). Fragmentation and Densities of Meteoroids. Astron. Ap., 384, 317-321.
4. Bailey, M., and Emelyanenko, V. (1996). Dynamical Evolution of Halley-Type Comets. MNRAS, 278, 1087-1110.
5. Bauer, J., Fernández, Y., and Meech, J. (2003). An Optical Survey of the Active Centaur C/NEAT (2001 T4). PASP., 115, 810, 981-989.
6. Bauer, J., Meech, K., Fernández, Y., Pittichova, J., Hainaut, O., Boehnhardt, H., and Delsanti, A. (2003). Physical Survey of 24 Centaurs with Visible Photometry. Icarus, 166, 195-211.

7. Bernstein, G., Trilling, D., Allen, R., Brown, M., Holman, M., and Malhotra, R. (2003). The Size Distribution of Trans-Neptunian Bodies. Astron. J., submitted.
8. Bertoldi, F., Altenhoff, W., and Junkes, N. (2002). Beyond Pluto: Max-Planck radioastronomers measure the sizes of distant minor planets. Max Planck Institute Press Release 10/02(2), 2002 October 7.
9. Blake, D., Allamandola, L., Sandford, S., Hudgins, D., and Friedemann, F. (1991). Clathrate Hydrate Formation in Amorphous Cometary Ice Analogs in Vacuo. Science 254, 548, 1991
10. Bottke, W., Morbidelli, A., Jedicke, R., Petit, J., Levison, H., Michel, P., and Metcalfe, T. (2002). Debiased Orbital and Absolute Magnitude Distribution of the Near-Earth Objects. Icarus, 156, 399-433.
11. Brin, G., and Mendis, D. (1979). Dust Release and Mantle Development in Comets. Ap. J., 229, 402-408.
12. Brown, P., and Jones, J. (1998). Simulation of the Formation of the Perseid Meteor Stream. Icarus, 133, 36-68.
13. Brunini, A., and Melita, M. (1998). On the Existence of a Primordial Cometary Belt between Uranus and Neptune. Icarus, 135, 408-414.
14. Burns, J. and Safronov, V. (1973). Asteroid nutation angles. MNRAS, 165, 403.
15. Bus, S., A'Hearn, M., Bowell, E. and Stern, S. (2001). (2060) Chiron: Evidence for Activity near Aphelion. Icarus, Volume 150, Issue 1, pp. 94-103 (2001)
16. Campins, H., and Fernández, Y. (2002). Observational constraints on Surface Characteristics of Cometary Nuclei. Earth Moon and Planets, 89, 117-134.
17. Catullo, V., Zappala, V., Farinella, P., and Paolicchi, P. (1984). Analysis of the Shape Distribution of Asteroids. Astron. Ap., 138, 464-468.
18. Chamberlin, A., McFadden, L., Schulz, R., Schleicher, D., and Bus, S. (1996). 4015 Wilson-Harrington, 2201 Oljato, and 3200 Phaethon: Search for CN Emission. Icarus, 119, 173-181
19. Chen, J., and Jewitt, D. (1994). On the rate at which comets split. Icarus, 108, 265-271.
20. Dahlgren, M., and Lagerkvist, C. (1995). A Study of Hilda Asteroids. Astron. Ap., 302, 907-914.
21. Degewij, J., and Tedesco, E. (1982). Do Comets Evolve Into Asteroids? In Comets, ed. L. L. Wilkening, Univ. Az. Press, Tucson, pp. 665-695.
22. Delsemme, A. (1973). Origin of the Short-period Comets. Astron. Ap., 29, 377-381.
23. Dones, L., Gladman, B., Melosh, H., Tonks, W., Levison, H. and Duncan, M.. (1999). Dynamical Lifetimes and Final Fates of Small Bodies. Icarus, 142, 509-524.
24. Dumas, C., Owen, T., and Barucci, M. (1998). Near-Infrared Spectroscopy of Low-Albedo Surfaces of the Solar System. Icarus, 133, 221-232.
25. Duncan, M., Quinn, T., and Tremaine, S. (1988). The Origin of Short Period Comets. Ap. J. L69-L73.
26. Fernández, J. A. (1980). On the existence of a comet belt beyond Neptune. MNRAS, 192, 481-491
27. Fernández, J. A., Tancredi, G., Rickman, H., and Licandro, J. (1999) The population, magnitudes, and sizes of Jupiter family comets. Astron. Ap., 352, 327
28. Fernández, J., Gallardo, T., and Brunini, A. (2002). Are There Many Inactive JFCs Among the Near Earth Asteroid Population? Icarus, 159, 358-368.
29. Fernández, Y. R., McFadden, L. A., Lisse, C. M., Helin, E. F., Chamberlin, A. B. (1997). Analysis of POSS Images of Comet-Asteroid Transition Object 107P/1949 W1 (Wilson-Harrington). Icarus, 128, 114-126.

30. Fernández, Y., Lisse, C., Ulrich K., Peschke, S., Weaver, H., A'Hearn, M., Lamy, P., Livengood, T., Kostiuk, T., (2000). Physical Properties of the Nucleus of Comet 2P/Encke. Icarus, 147, Issue 1, pp. 145-160
31. Fernández, Y., Jewitt, D., and Sheppard, S. (2001). Low Albedos Among Extinct Comet Candidates. Ap. J., 553, L197-L200.
32. Fernández, Y., Sheppard, S. and Jewitt, D. (2003). The Albedo Distribution of Jovian Trojan Asteroids. Astron. J., 126, 1563-1574.
33. Fernández, Y., Jewitt, D. and Sheppard, S. (2003). Albedos of Asteroids in Comet-Like Orbits. Submitted to Astron. J.
34. Fitzsimmons, A., Dahlgren,M., Lagerkvist,C, Magnusson,P., and Williams,I. (1994). A spectroscopic survey of D-type asteroids. Astron. Ap. 282, 634-642
35. Giblin, I., and Farinella, P. (1997). Tumbling Fragments from Experiments Simulating Asteroidal Catastrophic Disruption. Icarus, 127, 424-430.
36. Grün, E. and 23 others (2001). Broadband infrared photometry of comet Hale-Bopp with ISOPHOT. Astron. Ap., 377, 1098-1118.
37. Gutiérrez, P., Jorda, L., Ortiz, J. and Rodrigo, R. (2003). Long-term simulations of the rotational state of small irregular cometary nuclei. Astron. Ap., 406, 1123-1133
38. Hahn, J., and Malhotra, R. (1999). Orbital Evolution of Planets Embedded in a Planetesimal Disk. Astron. J., 117, 3041-3053.
39. Hainaut, O. R., Delsanti, A. C. (2002). Colors of Minor Bodies in the Outer Solar System. A statistical analysis. Astron. Ap., 389, 641-664.
40. Harris, A. (1994). Tumbling Asteroids. Icarus, 107, 209.
41. Harris, N., and Bailey, M. (1998). Dynamical Evolution of Cometary Asteroids. MNRAS, 297, 1227-1236.
42. Hartmann, W., Tholen, D., and Cruikshank, D. (1987). The relationship of active comets, 'extinct' comets, and dark asteroids. Icarus, Icarus 69, 33-50.
43. Hartmann, W. and Tholen, D. (1990). Comet nuclei and Trojan asteroids - A new link and a possible mechanism for comet splittings. Icarus, 86, 448-454.
44. Holman, M. (1997). A possible long-lived belt of objects between Uranus and Neptune. Nature, 387, 785-788.
45. Hsieh, H., Jewitt, D., and Fernández, Y. (2003). The Strange Case of 133P/Elst-Pizarro: A Comet Amongst the Asteroids. Submitted to Astron. J.
46. Hughes, D., and McBride, N. (1989). The Masses of Meteoroid Streams. MNRAS, 240, 73-79.
47. Ishiguro, M., Kwon, S., Sarugaku, Y., Hasegawa, S., Usui, F., Nishiura, S., Nakada, Y., Yano, H. (2003). Discovery of the Dust Trail of the Stardust Comet Sample Return Mission Target: 81P/Wild 2. Ap. J., 589, L101-L104.
48. Jenniskens, P., and Betlem, H. (2000). Massive Remnant of Evolved Cometary Dust Trail detected in the Orbit of Halley-Type Comet 55P/Tempel-Tuttle. Ap. J., 531, 1161-1167.
49. Jewitt, D. (1991), "Cometary Photometry", In Comets In The Post - Halley Era, eds. R. Newburn, M. Neugebauer and J. Rahe. Kluwer Academic Publishers, Netherlands. pp. 19 - 65.
50. Jewitt, D. (1996a). From Comets to Asteroids: When Hairy Stars Go Bald. Earth, Moon and Planets, 72, 185-201.
51. Jewitt, D. (1996b). Debris From Comet P/Swift-Tuttle. Astron. J. 111, 1713
52. Jewitt, D. (1999). Cometary Rotation: An Overview. Moon and Planets, 79, 35-53.
53. Jewitt, D. and Luu, J. (2001). Colors and Spectra of Kuiper Belt Objects. Astron. J., 122, 2099-2114.
54. Jewitt, D. (2002). From Kuiper Belt Object to Cometary Nucleus: The Missing Ultrared Matter. Astron. J., 123, 1039-1049.

55. Jewitt, D. and Meech, K (1988). Optical Properties of Cometary Nuclei and a Preliminary Comparison with Asteroids. Ap. J., 328, 974-986.
56. Jewitt, D., and Luu, J. (1990). CCD spectra of asteroids. II - The Trojans as spectral analogs of cometary nuclei. Astron. J., 100, 933-944.
57. Jewitt, D., and Kalas, P. (1998). Thermal Observations of Centaur 1997 CU26. Ap. J. 499, L103
58. Jewitt, D., Trujillo, C. and Luu, J. (2000). "Population and Size Distribution of Small Jovian Trojan Asteroids". Astron. J., 120, 1140-1147.
59. Jewitt, D., Aussel, H. and Evans, A. (2001). The size and albedo of the Kuiper-belt object (20000) Varuna. Nature, 411, 446-447.
60. Jewitt, D. and Fernández, Y. (2001). Physical Properties of Planet-Crossing Objects. In Collisional Processes in the Solar System. ed. H. Rickman and M. Marov. Astrophysics and Space Science Library Series, Kluwer Academic Publishers, Dordrecht, pp. 143-161.
61. Jewitt, D., Sheppard, S., and Fernández, Y. (2003). 143P/Kowal-Mrkos and the Shapes of Cometary Nuclei. Astron. J., 125, 3366-3377.
62. Jones, T., Lebofsky, L., Lewis, J., and Marley, M. (1990). The composition and origin of the C, P, and D asteroids - Water as a tracer of thermal evolution in the outer belt. Icarus, 88, 172-192.
63. Kresak, L. (1987). Dormant Phases in the Aging of Periodic Comets. Astron. Ap., 187, 906-908.
64. Kührt, E., and Keller, H. U. (1994). The formation of cometary surface crusts. Icarus, 109, 121-132.
65. Lamy, P., Toth, I., Fernández, Y., and Weaver, H. (2004). This volume.
66. Levison, H. (1996). In "Completing the Inventory of the Solar System", Astron. Soc. Pacific Conference Series 107, 173-191.
67. Levison, H. F., Morbidelli, A., Dones, L., Jedicke, R., Wiegert, P. A., and Bottke, W. F. (2002). The Mass Disruption of Oort Cloud Comets. Science, 296, 2212-2215.
68. Levison, H., and Duncan, M. (1994). The long-term dynamical behavior of short-period comets. Icarus, 108, 18-36.
69. Levison, H., and Duncan, M. (1997). From the Kuiper Belt to Jupiter Family Comets: The Spatial Distribution of Ecliptic Comets. Icarus, 127, 13-32.
70. Levison, H., Dones, L., and Duncan, M. (2001). The Origin of Halley-Type Comets: Probing the Inner Oort Cloud. Astron. J., 121, 2253-2267.
71. Lissé, C., Fernández, Y., Kundu, A., A'Hearn, M., Dayal, A., Deutsch, L., Fazio, G., Hora, J., and Hoffmann, W. (1999). The Nucleus of Comet Hyakutake (C/1996 B2). Icarus, 140, 189-204.
72. Luu, J., and Jewitt, D. (1992). High resolution surface brightness profiles of near-earth asteroids. Icarus, 97, 276-287.
73. Luu, J., and Jewitt, D. (1992). Near-Aphelion CCD Photometry of Comet P/Schwassmann Wachmann 2, Astron. J., 104, 2243-2249.
74. Luu, J., Jewitt, D., Cloutis,E. (1994). Near-infrared spectroscopy of primitive solar system objects. Icarus 109, 133-144
75. Marchi, S., Lazzarin, M., Magrin, S., and Barbieri, C. (2003). Visible Spectroscopy of the Two Largest Known Trans-Neptunian Objects. Astron. Ap., 408, L17-L19.
76. Marzari, F., Farinella, P., and Vanzani, V. (1995). Are Trojan collisional families a source for short-period comets? Astron. Ap., 299, 267.
77. Moroz, L., Starukhina, L., Strazzulla, G., Baratta, G., Dotto, E., Barucci, A., and Arnold, G. (2003). Optical Alteration of Complex Organics Caused by Ion Irradiation. Icarus, in press.

78. Oort, J. (1950). The Structure of the Cloud of Comets Surrounding the Solar System and a Hypothesis Concerning its Origin. Bull. Astron. Inst. Netherlands, 11, 91-110.
79. Pittich, E., and Rickman, H. (1994). Cometary Splitting - A Source for the Jupiter Family? Astron. Ap., 281, 579-587.
80. Pravec, P., Harris, A., and Michalowski, T. (2002). In Asteroids III, ed. W. Bottke et al, Univ. Az. Press, Tucson, pp 113-122.
81. Rabinowitz, D., Helin, E., Lawrence, K., and Pravdo, S. (2000). A Reduced Estimate of the Number of Kilometer-Sized Near-Earth Asteroids. Nature, 402, 165-166.
82. Reach, W., Sykes, M., Lien, D., and Davies, J. (2000). The Formation of Encke Meteoroids and Dust Trail. Icarus, 148, 80-94.
83. Rickman, H., Fernández, J. A., Gustafson, B. A. S. (1990). Formation of stable dust mantles on short-period comet nuclei. Astron. Ap., 237, 524-535.
84. Rickman, H., Valsecchi, G. B., and Froeschl, Cl. (2002). From the Oort cloud to observable short-period comets - I. The initial stage of cometary capture. MNRAS, 325, 1303-1311.
85. Rubio, L., Gonzalez, M., Herrera, L., Licandro, J., Delgado, D., Gil, P. and Serra-Ricart, M. (2002). Modelling the Photometric and Dynamical Behavior of Super-Schmidt Meteors in the Earth's Atmosphere. Astron. Ap., 389, 680-691.
86. Samarasinha, N. (2001). A Model for the Breakup of Comet LINEAR (C/1999 S4). Icarus, 154, 540-544.
87. Samarasinha, N., A'Hearn, M., Hoban, S., and Klinglesmith, D., (1986). CN jets of Comet P/Halley: Rotational properties. In ESA Proceedings of the 20th ESLAB Symposium on the Exploration of Halley's Comet. Volume 1: Plasma and Gas p 487-491.
88. Samarasinha, N. H., and A'Hearn, M. F. (1991). Observational and Dynamical Constraints on the Rotation of Comet P/Halley. Icarus, 93, 194-225.
89. Sekanina, Z. (1990). Gas and dust emission from comets and life spans of active areas on their rotating nuclei. Astron. J., 100, 1293-1314.
90. Sekanina, Z. (1997). The Problem of Split Comets Revisited. Astron. Ap., 318, L5-8.
91. Sekanina, Z. (2002). Statistical Investigation and Modeling of Sungrazing Comets Discovered with the Solar and Heliospheric Observatory. Ap. J., 566, 577-598.
92. Sheppard, S., Jewitt, D., Trujillo, C., Brown, M., and Ashley, M. (2000). A Wide Field CCD Survey for Centaurs and Kuiper Belt Objects. Astron. J., 120, 2687-2694.
93. Shul'man, L. (1972). The Chemical Composition of Cometary Nuclei. In The Motion, Evolution of Orbits and Origin of Comets. IAU Symp. 45, eds. G. Chebotarev, E. Kazimirchak-Polonskaya and B. Marsden. p. 265-270. Reidel Pub. Co., Dordrecht, The Netherlands.
94. Stern, S. (1995). Collisional Time Scales in the Kuiper Disk and Their Implications. Astron. J., 856
95. Stern, S. and Weissman, P. (2001). Rapid collisional evolution of comets during the formation of the Oort cloud. Nature, 409, 589-591.
96. Sykes, M., and Walker, R. (1992). Cometary dust trails. I - Survey. Icarus, 95, 180-210.
97. Tancredi, G. (1995). The Dynamical Memory of Jupiter Family Comets. Astron. Ap. 299, 288-292.
98. Tedesco, E. Noah, Paul V., Noah, Meg, Price, Stephan D. (2002) The Supplemental IRAS Minor Planet Survey. Astron. J., 123, 1056-1085.

99. Tholen, D., and Buie, M. (1997). Bulk Properties of Pluto and Charon. In Pluto and Charon, eds. S. A. Stern and D. J. Tholen, Univ Az. Press, Tucson, pp. 193-220.
100. Toth, I. (2000). Impact Generated Activity Period of the Asteroid 7968 Elst-Pizzaro in 1996. Astron. Ap., 360, 375-380.
101. Trujillo, C., Jewitt, D., and Luu, J. (2001). Properties of the Trans-Neptunian Belt: Statistics from the Canada-France-Hawaii Telescope Survey. Astron. J., 122, 457-473.
102. Weaver, H. et al. (2001). HST and VLT Investigations of the Fragments of Comet C/1999 S4 (LINEAR). Science, 292, 1329-1334.
103. Weissman, P. (1980). Physical loss of long-period comets. Astron. Ap., 85, 191-196.
104. Weissman, P. R. and Lowry, S. C. (2003), Lunar and Planet. Sci. XXXIV, abstract no. 2003.
105. Weissman, P., Bottke, W., and Levison, H. (2002). Evolution of Comets into Asteroids. In Asteroids III, eds. W. Bottke, A. Cellino, P. Paolicchi and R. Binzel, Univ. Az. Press, Tucson.
106. Whipple, F. (1950). A Comet Model: I. The Acceleration of Comet Encke. Ap. J., 111, 375-394.
107. Wiegert, P., and Tremaine, S. (1999). The Evolution of Long-Period Comets. Icarus, 137, 84-121.
108. Williams, I., and Collander-Brown, S. (1998). The Parent of the Quadrantids. MNRAS, 294, 127-138.